Multiscale dynamical analysis of a high-resolution numerical model simulation of the Solomon Sea circulation

Bughsin' Djath, Jacques Verron, Angélique Mélet, Lionel Gourdeau, Bernard Barnier, Jean-Marc Molines

AGU PUBLICATIONS

JGR

Journal of Geophysical Research: Oceans

RESEARCH ARTICLE

10.1002/2013JC009695

Special Section:
Western Pacific Ocean Circulation and Climate

Multiscale dynamical analysis of a high-resolution numerical model simulation of the Solomon Sea circulation

Bughsin' Djath[1], Jacques Verron[1], Angelique Melet[2], Lionel Gourdeau[3], Bernard Barnier[1], and Jean-Marc Molines[1]

[1]CNRS, LGGE, Grenoble, France, [2]Program in Atmospheric and Oceanic Sciences, Princeton University, Princeton, New Jersey, USA, [3]IRD, LEGOS, Toulouse, France

Key Points:
- The 1/36° numerical simulations of the Solomon Sea circulations are analyzed
- The levels of eddy kinetic energy are drastically increased
- The emergence of submesoscales is apparent and analyzed with spectral tools

Correspondence to:
B. Djath,
bughsin.djath@legi.grenoble-inp.fr

Citation:
Djath, B., J. Verron, A. Melet, L. Gourdeau, B. Barnier, and J.-M. Molines (2014), Multiscale dynamical analysis of a high-resolution numerical model simulation of the Solomon Sea circulation, *J. Geophys. Res. Oceans*, *119*, 6286–6304, doi:10.1002/2013JC009695.

Received 16 DEC 2013
Accepted 14 JUL 2014
Accepted article online 17 JUL 2014
Published online 18 SEP 2014

Abstract A high 1/36° resolution numerical model is used to study the ocean circulation in the Solomon Sea. An evaluation of the model with (the few) available observation shows that the 1/36° resolution model realistically simulates the Solomon Sea circulations. The model notably reproduces the high levels of mesoscale eddy activity observed in the Solomon Sea. With regard to previous simulations at 1/12° resolution, the average eddy kinetic energy levels are increased by up to ∼30–40% in the present 1/36° simulation, and the enhancement extends at depth. At the surface, the eddy kinetic energy level is maximum in March-April-May and is minimum in December-January-February. The high subsurface variability is related to the variability of the western boundary current (New Guinea Coastal Undercurrent). Moreover, the emergence of submesoscales is clearly apparent in the present simulations. A spectral analysis is conducted in order to evidence and characterize the modeled submesoscale dynamics and to provide a spectral view of scales interactions. The corresponding spectral slopes show a strong consistency with the Surface Quasi-Geostrophic turbulence theory.

1. Introduction

The Solomon Sea is a choke point for the Low Latitude Western Boundary Currents (LLWBC) along their pathways from the subtropics to the equator. The LLWBCs especially include the surface New Guinea Coastal Current (NGCC) and the subsurface New Guinea Coastal Undercurrent (NGCU). These Solomon Sea currents are believed to be major contributors to the Equatorial Undercurrent (EUC) [*Tsuchiya*, 1981; *Tsuchiya et al*., 1989]. A change in mass or heat transport of the LLWBCs have the potential to impact the properties of the EUC, sea surface temperature (SST) in the equatorial Pacific, and modulate ENSO (El Niño Southern Oscillation) events at low frequency [*Fedorov and Philander*, 2001; *Sun et al*., 2004; *Chang et al*., 2006]. Recently, *Melet et al*. [2011, 2013] showed that water masses modifications were occurring in the Solomon Sea. Therefore, the Solomon Sea is a key western boundary connection between the subtropics and the equator in the Pacific Ocean. In addition to raising several oceanographic climate-related questions, the Solomon Sea also represents an interesting region for studies aiming at a better description and understanding of LLWBC dynamics.

The Solomon Sea has been sparsely observed because of its remote location. Available in situ historical observations in this region are scarce and scattered in time and do not provide a complete coverage of the mean circulation or its variability [*Lindstrom et al*., 1990; *Murray et al*., 1995]. However, recent observations start to provide a much better observational picture of the Solomon Sea circulations [*Cravatte et al*., 2011; *Hristova and Kessler*, 2011; *Gasparin et al*., 2012; *Davis et al*., 2012]. Observations from space have shown that the sea surface height (SSH) and surface eddy kinetic energy (EKE) in the Solomon Sea area exhibit the highest variability of the whole south tropical Pacific Ocean. However, in the presence of complex coastal features such as in the Solomon Sea region, standard altimeter products fail to provide an accurate and extensive description and must be specifically retreated [*Melet et al*., 2010a].

The development of high-resolution regional numerical models represents a complementary strategy to study the Solomon Sea. For example, *Melet et al*. [2010b] gave the first description of the synoptical Solomon Sea circulation at thermocline level using a 1/12° resolution numerical model. The Solomon Sea is characterized by a complex bathymetry, with numerous straits (mainly Vitiaz Strait, St George's Channel,

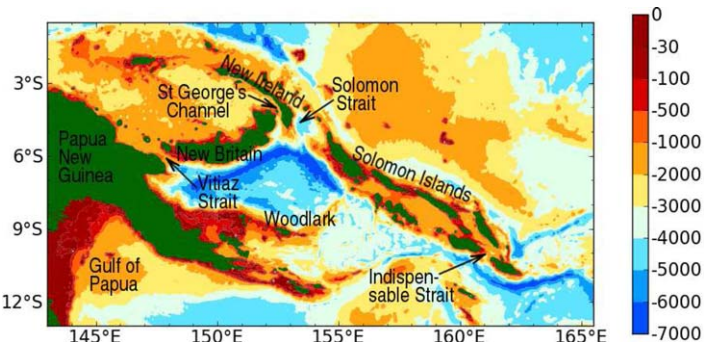

Figure 1. Geography and bathymetry of the Solomon Sea (depth in m).

Solomon Strait, and Indispensable Strait) and islands (Figure 1). From a modeling perspective, this raises the ever challenging issue of faithfully representing the topography and its impact on circulations. Therefore, using a high resolution in numerical simulations of the Solomon Sea is a key factor for the quality of the model results. In addition, the increase in model resolution allows access to smaller dynamical scales. The ubiquitous presence of eddies in the world ocean has now been well recognized notably, thanks to altimetry [*Morrow and Le Traon*, 2012]. The strongly turbulent dynamics of the ocean has been less studied in low-latitude regions than in the midlatitude jet systems. However, it is believed that eddy activity is also of key importance in the LLWBCs, such as these flowing within the Solomon Sea, and deserves further consideration.

Recent altimetric observations, such as these provided by the SARAL/AltiKa satellite launched in February 2013, give a refined along-track resolution that allows a better access to finer dynamical scales [*Verron*, 2013]. Even more importantly, the future SWOT (Surface Water and Ocean Topography) mission is expected to provide unprecedented 2-D high-resolution altimetric data that will resolve more small scale physics [*Fu et al*., 2009]. The key question of what ocean dynamical features will be observed by these altimetric satellites arises (the satellite observability question). A related question is how can high-resolution models help to apprehend and anticipate the answer to the satellite observability question?

In many ways, the present work contributes to the CLIVAR/Southwest Pacific Ocean and Climate Experiment, whose role is to understand the southwest Pacific Ocean circulation and its influence on regional and basin-wide climate through a combination of dedicated observational and modeling efforts (A. Ganachaud et al., Southwest Pacific Ocean Circulation and Climate Experiment (SPICE), submitted to *Journal of Geophysical Research: Oceans*, 2014). In a broader context, the present study also gives attention to the Solomon Sea's strongly unstable LLWBCs and associated turbulent activity.

To address those issues, a high-resolution (1/36°) model is used. The increase in resolution compared to previous regional models of the Solomon Sea is expected to provide a more realistic simulation of the circulations, a more adequate resolution of all the bathymetric/coastal features of the region, and a first look at submesoscale dynamics. Indeed, while the choice of the 1/36° resolution is primarily determined by computing resources and technical constraints, it is also seen as the resolution that will properly solve mesoscale processes (in particular, based on the concept of effective resolution [*Marchesiello et al*., 2011]) and will allow a first access to the submesoscales. The model configuration used in this study can therefore be considered as truly "eddy-resolving" and preliminarily "submesoscale-permitting."

The paper is organized as follows. A short description of the model is presented in section 2. Section 3 focuses on the description of the general circulations provided by the high-resolution model, and its comparison to some available observations. It also includes the description of the model results in key areas of the Solomon Sea. Section 4 discusses the mesoscale variability with a focus on the mean eddy kinetic energy and its seasonal cycle. Section 5 focuses on smaller scales and scale interactions through the analysis of SSH, SST, and KE wave number spectra as well as kinetic energy spectral fluxes. Finally, conclusions are given in section 6.

2. Modeling Approach

The numerical model of the Solomon Sea used in this study has a 1/36° horizontal resolution. This 1/36° resolution model is two-stage embedded into a global 1/12° ocean model developed in the DRAKKAR project (www.ifremer.fr/lpo/drakkar): (i) From this global model, a 1/12° basin scale model of the southwest Pacific is selected and one-way controlled using an open boundary strategy [*Tréguier et al*., 2001]. (ii) The

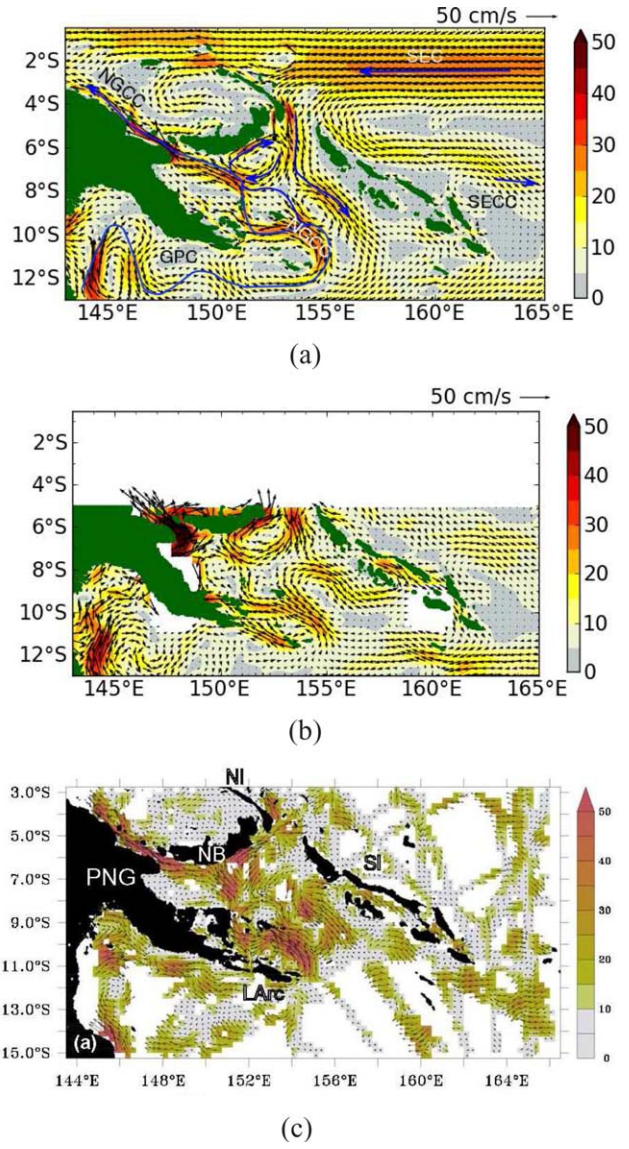

Figure 2. Mean surface circulation (in cm s^{-1}) over 1993–2007 in the Solomon Sea (a) from the 1/36° model at 10 m, (b) from AVISO data, and (c) from SADCP data [*Cravatte et al.*, 2011]. The currents amplitudes (shading) are in cm s^{-1}.

1/36° is then two-way (i.e., interactively) embedded in the previous southwest Pacific model using the AGRIF software [*Debreu et al.*, 2008].

The numerical code is based on the oceanic component of the NEMO (Nucleus for European Modelling of the Ocean) system [*Madec*, 2008]. The model formulation is based on standard primitive equations. The equations are discretized on the classical isotropic Arakawa C grid using a Mercator projection. The vertical coordinate is geopotential, and 46 vertical levels are prescribed from the surface down to 5875 m. At the lateral boundaries, a partial slip boundary condition is applied [*Djath et al.*, 2014]. A partial step parameterization, allowing bottom cells depth to be adaptive, is used to improve the bathymetry representation [*Adcroft et al.*, 1997; *Barnier et al.*, 2006]. The bathymetry of the high-resolution Solomon Sea model is based on the GEBCO08 data set. Atmospheric boundary conditions, consisting in surface fluxes of momentum, heat, and freshwater, are diagnosed through classical bulk formulas [*Large and Yeager*, 2009]. Wind and atmospheric temperature and humidity are provided from the ERA Interim reanalysis [*Dee et al.*, 2011]. The regional models were initialized with the climatological mass field of the World Ocean Atlas [*Levitus et al.*, 1998] and were integrated from 1989 to 2007. A spin-up phase of 4 years is allowed and the simulations are analyzed over the 1993–2007 year range. Output fields consist of daily means, which provides 164 Gb of data per simulated year. It must be stated that in such a configuration, each state variable of the model has $\sim 2 \times 10^7$ degrees of freedom. Handling and analyzing the simulations proved to be heavy tasks.

More technical details on the configuration of this model may be found in *Djath et al.* [2014].

3. General Circulation

3.1. Surface and Thermocline Circulations

The mean surface circulation computed over the whole 1993–2007 simulation period is shown in Figure 2a. The Solomon Sea circulations are fed by the large scale westward inflow from the South Equatorial Current

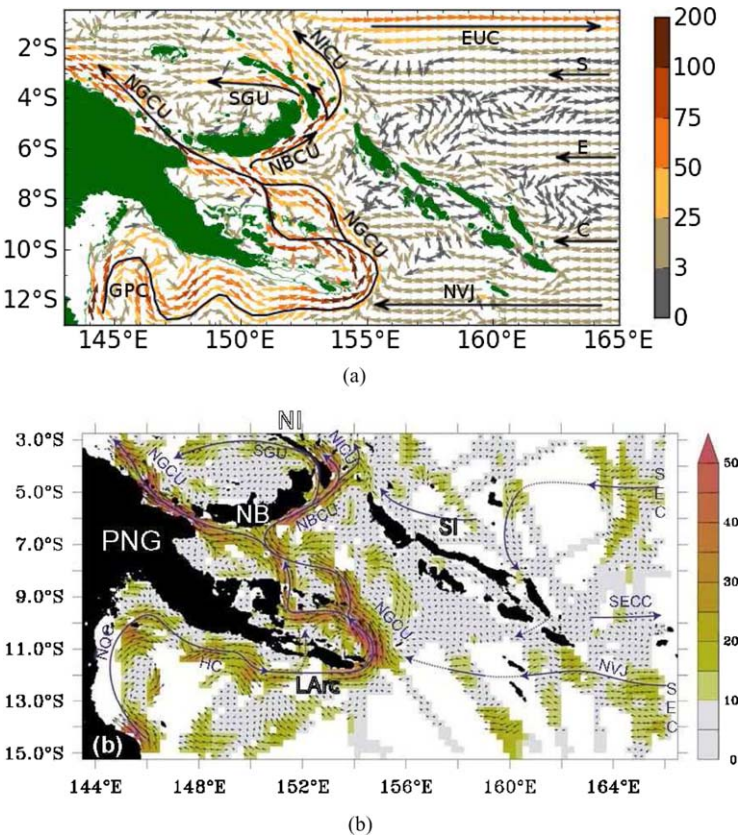

Figure 3. Mean circulation over 1993–2007 in the Solomon Sea integrated in the thermocline over $\sigma = 24-26.5 \mathrm{kg/m^3}$ (in $\mathrm{m^2 s^{-1}}$), (a) from the 1/36° model and (b) from SADCP data (in cm $\mathrm{s^{-1}}$) [*Cravatte et al.*, 2011].

(SEC), with inflows from both the Coral Sea and through Solomon Strait, and by the equatorward Gulf of Papua Current (GPC) [*Ganachaud et al.*, 2013] [e.g., *Fine et al.*, 1994; *Cravatte et al.*, 2011; *Melet et al.*, 2013]. Within the Solomon Sea, the surface circulation is mostly characterized by the northward New Guinea Coastal Current (NGCC). The NGCC mostly exits the Solomon Sea through Vitiaz Strait. In the northern Solomon Sea, south of the island of New Britain, a specific quasipermanent loop circulation is created in the surface layers by the encountering of the southward SEC inflow through Solomon Strait with the northward NGCC.

This surface model circulation is similar to the geostrophic surface circulation computed from the AVISO altimetric database (Figure 2b). However, the AVISO gridded data are provided on a 1/3° resolution grid. Maybe more significantly, the surface model circulation is quite analogous to that obtained from the compilation of historical SADCP observations by *Cravatte et al.* [2011] (Figure 2c).

Subsurface thermocline circulation (Figure 3a) is computed within the $\sigma = 24-26.5 \mathrm{kg/m^3}$ isopycnal range (corresponding to a depth range of approximately 100–400 m). This depth range is of major interest since it encompasses the South Pacific LLWBCs cores. At thermocline level, the mean GPC forms a large meander south of the Papua New Guinea before entering into the Solomon Sea. The GPC current joins with the North Vanuatu Jet (NVJ) around 155°E to feed the NGCU. The NGCU then flows equatorward toward Vitiaz Strait. South of the island of New Britain, the NGCU divides into a branch flowing through Vitiaz Strait and along the northern coast of Papua New Guinea (still called NGCU), and into a branch flowing eastward south of New Britain, called the New Britain Undercurrent (NBCU). This corroborates the existence of the NBCU, first identified by *Melet et al.* [2010b]. Although less marked than at the surface, a recirculation loop is also simulated at thermocline level south of the NBCU. This recirculation pattern can be attributed to the westward inflow through Solomon Strait and the northeastward NBCU. The NBCU exits the Solomon Sea through both St George's Channel and Solomon Strait. The NBCU outflow through St George's Channel forms the St

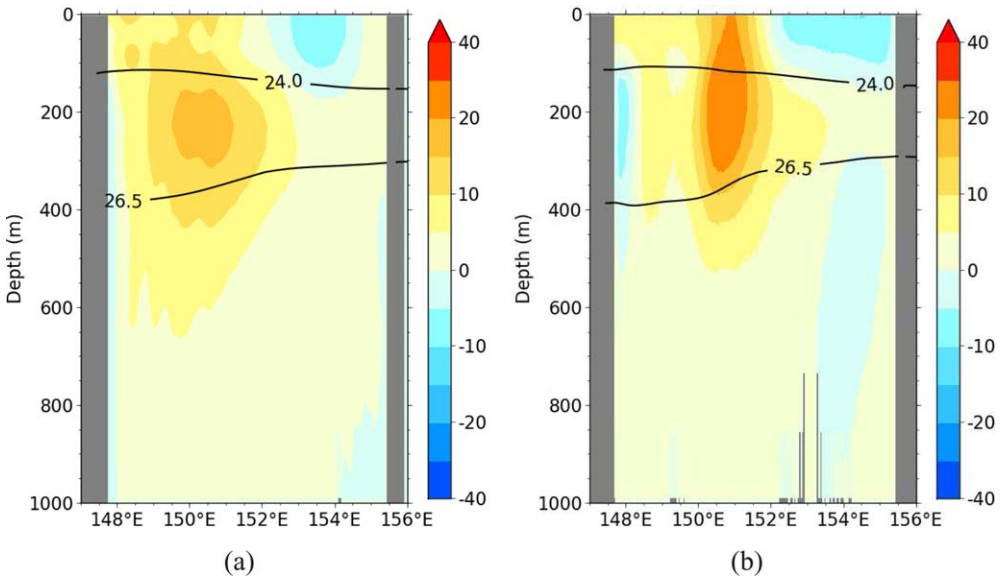

Figure 4. Geostrophic velocity section at 7.4°S (a) from CARS climatology and (b) from the 1/36° model. Unit: cm s^{-1}.

George's Channel Undercurrent (SGU) [*Lindstrom et al*., 1990; *Melet et al*., 2010b]. The NBCU outflow through Solomon Strait feeds (together with the SEC) the New Ireland Coastal Undercurrent (NICU), flowing equatorward along the island of New Ireland, consistently with the observations by *Butt and Lindstrom* [1994] and *Kessler and Gourdeau* [2007], and with the model study by *Melet et al*. [2010b].

This thermocline model circulation pattern is very close to the SADCP observations from *Cravatte et al*. [2011] (Figure 3b) in the range of 100–300 m and for the main features with the numerical model results by *Melet et al*. [2010b].

On its northward route, the NGCU is subdivided into two branches upstream of the Woodlark Island, flowing along each side of the island and rejoining downstream at around 152°E, 8°S. This double circulation around the Woodlark Island is in good agreement with the observed SADCP data [*Cravatte et al*., 2011]. It was not observed in the numerical simulation by *Melet et al*. [2010b] that used a free-slip lateral boundary condition. Sensitivity experiments to the lateral boundary conditions, using either free-slip, no-slip, or partial slip were carried out in *Djath et al*. [2014]. They show that using a partial slip boundary condition, as in the present study, significantly improves the 1/12° model behavior. In addition to the choice of lateral boundary conditions, the 1/36° resolution brings more refinement to the way the flow is controlled by the bathymetry. The impact of the use of a 1/36° resolution on the flow/bathymetry interaction can be seen not only in the Woodlark Islands region, but also in many locations in the Solomon Sea basin (e.g., for the detailed current structure in the St George's Channel and other small straits or for the effects of several seamounts).

On the eastern side of the Solomon Sea, at thermocline level, only a weak equatorward coastal flow is simulated along the Solomon Islands. The presence of the Solomon Islands Coastal Undercurrent (SICU) reported in the 1/12° numerical model by *Melet et al*. [2010b] is significantly less marked in our simulation. Further consideration on the hypothetical SICU is provided in section 3.4.

3.2. Vertical Structure

The modeled T, S, and geostrophic velocity properties have been compared to the CARS (CSIRO Atlas of Regional Seas) climatology [*Ridgway et al*., 2002] within the Solomon Sea through the 7.4°S section. Regarding the velocity fields shown in Figure 4, the model geostrophic currents are compared to the observed CARS climatology ones relative to 1100 m. There is a good general consistency between the 1/36° model and the climatology although the NGCU is significantly more intense in the model than in CARS. However, the comparison is of limited scope as the CARS climatology has a rather coarse resolution.

Comparison with in situ measurements from the FLUSEC campaign [*Maes et al*., 2009] has been made over all the available profiles. Although such profiles are clearly of specific focus in time and space, they are

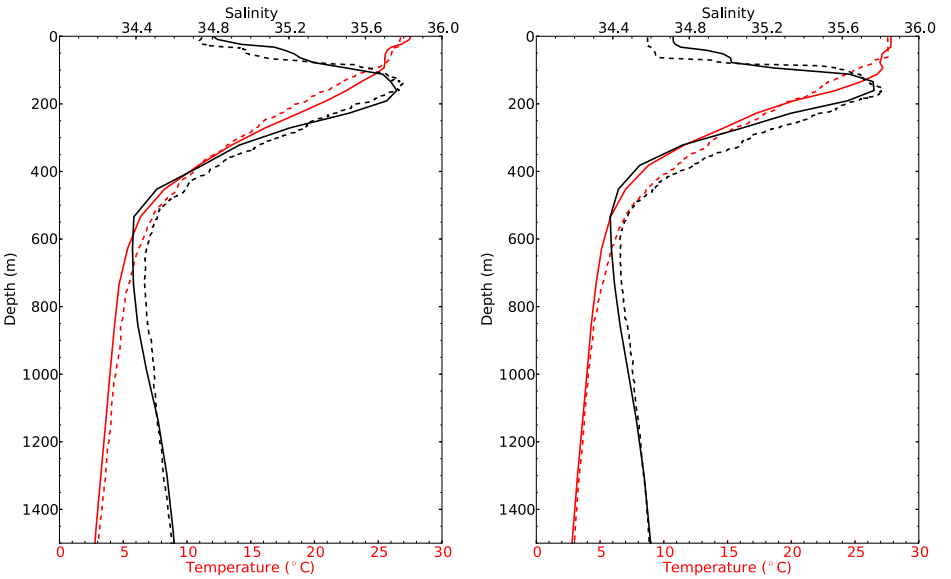

Figure 5. Temperature and salinity profiles from the FLUSEC cruise (dashed line) and from the 1/36° model (full line) at (a) 154°56.61′E, 11°36.63′S and (b) 155°55.82′E, 11°06.95′S on 19 August 2007.

indicative of the model performances. Two examples are shown in Figure 5 where the temperature and salinity model profiles are colocalized and compared with two FLUSEC CTD profiles (note that comparisons for other profiles provide similar good results). The modeled T, S profiles are close to the observed ones in the surface and thermocline layers (the differences between the observed and modeled temperature/salinity are smaller than 1°C and 0.1 psu). Slightly larger differences (∼2°C and 0.2 psu) are found in the intermediate layers, in the 400–600 m depth range.

Another assessment of the model against observations is provided using the XBT database from the "Ships of Opportunity" that has been collected by IFREMER and analyzed in the southwest Pacific region by *Kessler and Cravatte* [2013]. Comparison of the modeled and observed interannual variability of the temperature field is shown in Figure 6 along the Solomon Sea portion (11°S–5°S) of the Auckland-Solomon Strait transect. The vertical distribution of the 1993–1999 interannual temperature anomalies is quite consistent between the observations and the model.

3.3. Currents at Straits

As indicated earlier, the control of the flow by the various straits of Solomon Sea is a key aspect of the Solomon Sea circulation that deserves specific considerations. Examining the flow through main straits of the Solomon Sea also provides key information to understand the western boundary pathways from the SEC to the equator.

3.3.1. Vitiaz Strait

WEPOCS campaigns [*Lindstrom et al*., 1987, 1990] and SADCP data [*Cravatte et al*., 2011] provided detailed observations of currents through Vitiaz Strait and St George's Channel. In these in situ data, the core of the NGCU is found in the thermocline between ∼100 and 250 m and reaches velocity of 70–110 cm s^{-1}. In the 1/36° model simulation, the mean currents show that the core of the NGCU at Vitiaz Strait is found between 150 and 300 m with speeds of 90–100 cm s^{-1} (Figure 7a), in good agreement with observations.

The mean modeled top-to-bottom transport through Vitiaz Strait is 13.8 Sv for the 1993–2007 period. In the 0–300 m depth range, the modeled transport is about 8.9 Sv, compared to 7.4 Sv for SADCP observations [*Cravatte et al*., 2011]. More than two-thirds of the total transport through Vitiaz Strait occurs within the thermocline.

The seasonal cycle of the transport through Vitiaz Strait shows a maximum in July to August and a minimum in February to April. But this transport also has a significant interannual variability (Figure 7b).

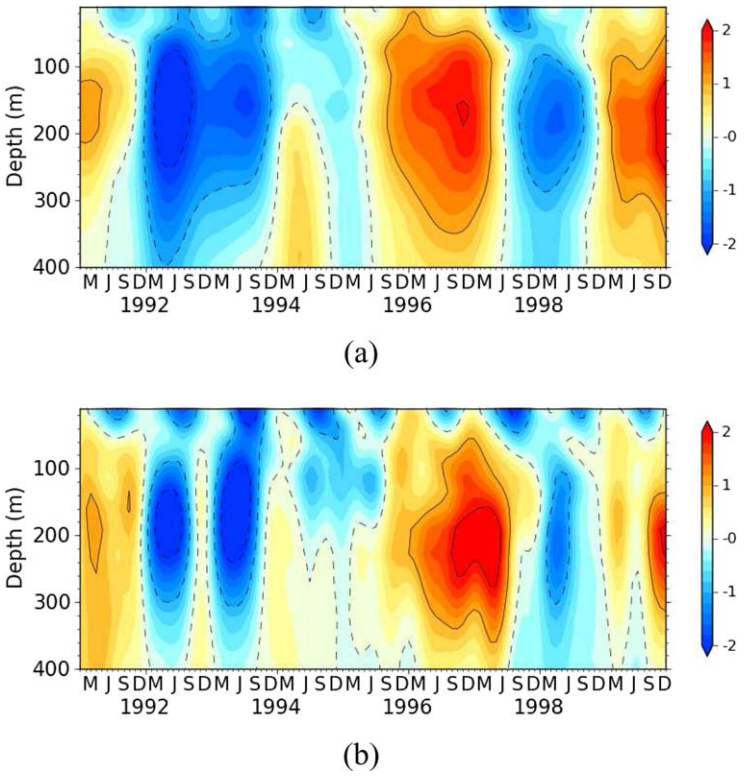

Figure 6. The 1993–1999 interannual variation of the temperature anomaly over the (11°S–5°S) range of the Auckland-Solomon Strait XBT transect from the XBT observations (a) from *Kessler and Cravatte* [2013] and (b) from the high-resolution model. Unit: °C.

3.3.2. St George's Channel

As previously said, currents transiting through St George's Channel feed the SGU, which eventually reconnects to the NGCU and the EUC (Figure 2b) in agreement with earlier studies of *Lindstrom et al*. [1990]. At St George's Channel, the core of the northward flow through St George's Channel is located between ∼100 and 300 m, with the velocities of about 40 cm s^{-1} (Figure 7c). The flow is vertically sheared: a southward surface flow is superimposed to the previous northward flow below 100 m depth. This is an interesting situation that is liable for marked instabilities (a clear EKE signature can be seen at this specific location in Figure 10a). The mean depth-integrated northward transport is about 2.8 Sv. In the 0–300 m depth range, the modeled transport is 2 Sv while it is 1.5 Sv in *Cravatte et al*. [2011].

As displayed in Figure 7d, the transport through St George's Channel exhibits a strong seasonal cycle and not a so well marked interannual variability. The transport is maximum in April to June and minimum in October to November. As was the case in Vitiaz Strait, the maximum transport is located between 100 and 400 m, which represents 2.6 Sv, more than 90% of the total transport.

3.3.3. Solomon Strait

The vertical structure of the flow through Solomon Strait is also strongly sheared in the first 300 m (Figure 7e). The surface currents in the first 100 m are negative, i.e., they flow poleward inside the Solomon Sea. This corresponds to the SEC inflow through Solomon Strait. At thermocline depth (between 100 and 300 m depth) the flow is equatorward and corresponds to the northeastward NBCU flowing out of the Solomon Sea. Between the surface and 300 m depth, the average transport through Solomon Strait is 4.6 Sv. This is in agreement with SADCP data that measured a transport of 4.2 Sv [*Cravatte et al*., 2011] although SADCP are probably less reliable than elsewhere in this area where the space/time variability is strong. The thermocline transport is minimum in March (4 Sv) and maximum in August (8 Sv) and a significant interannual variability is observed (Figure 7f).

A southward current core is noticeable below 1000 m depth (not shown). It is more intense (∼20 cm s^{-1}) in December-January-February and minimum in June-July-August.

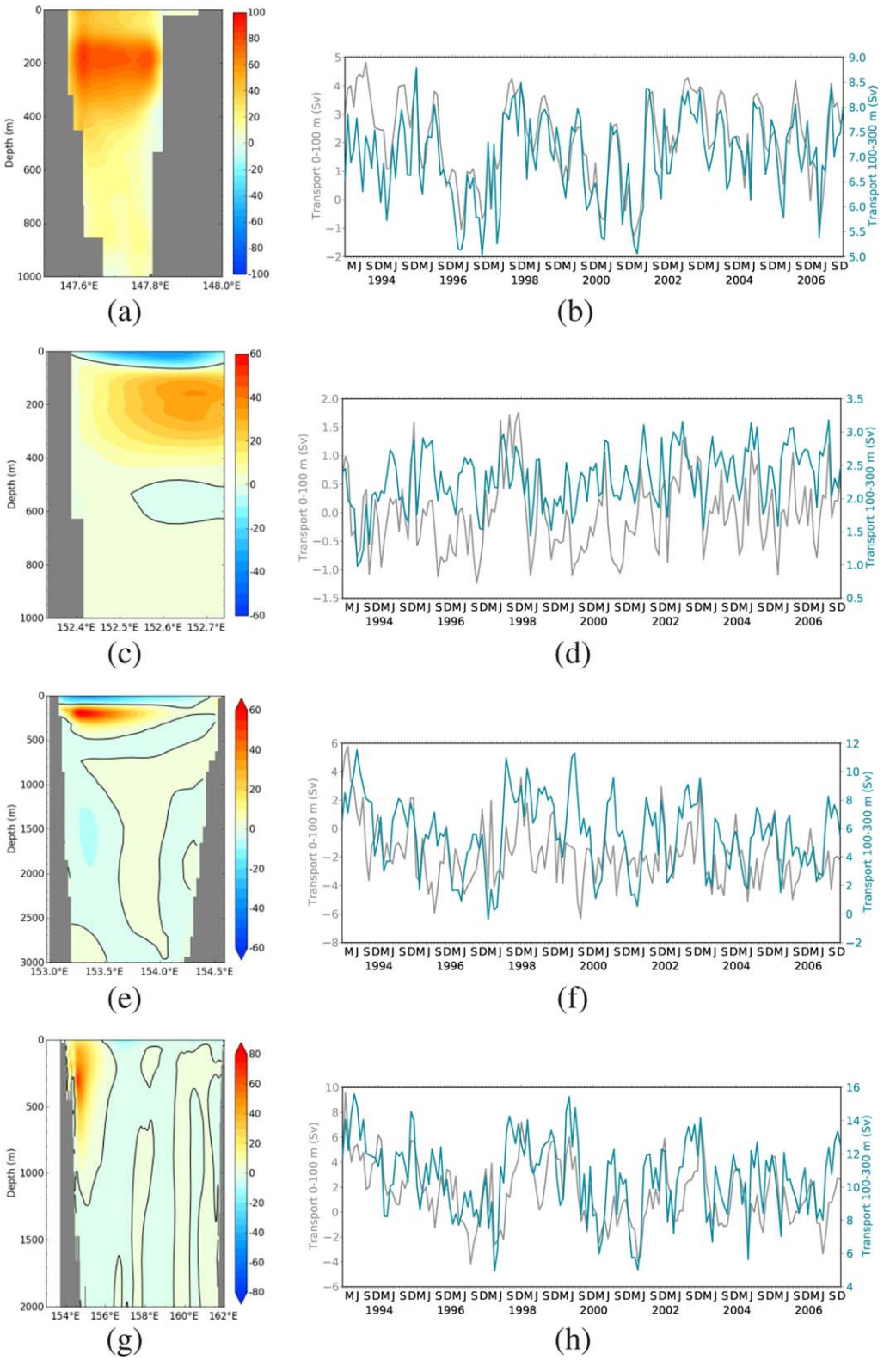

Figure 7. Mean velocity (in cm s^{-1}) from 1993 to 2007 section and time evolution of the transports (in Sv) at (a and b) Vitiaz Strait, (c and d) St George's Channel, (e and f) Solomon Strait, and (g and h) through the southern Solomon Sea section.

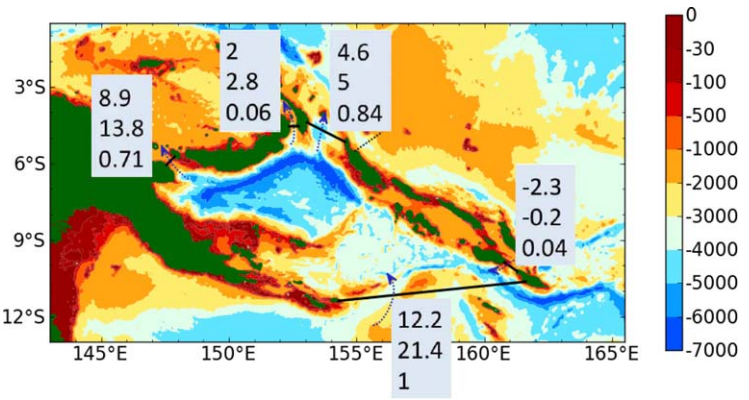

Figure 8. Model transport estimates in the main Solomon Sea straits (Vitiaz Strait, St George's Channel, Solomon Strait, and Indispensable Strait) and through the southern section: 0–300 m transport, full depth transport (Unit: Sv). The third numbers show the correlations between the southern section transport and the thermocline transports within the corresponding strait. The blue arrows indicate the direction of the transport.

3.3.4. South Entrance of the Solomon Sea

The inflow through the open south entrance of the Solomon Sea is crucial because it is through this area that most of the water of subtropical origin advected by the SEC transit before joining the equatorial region through the northern straits of the Solomon Sea.

The meridional section from Rossel Island (located at the eastern tip of the Lousiade Archipelago) to the southern tip of the Solomon islands encompasses both the NGCU western boundary current flowing northward and extending to more than 1000 m with a core located between 200 and 400 m (Figure 7g). The overall mean transport simulated by the model through this south Solomon Sea section is 21 Sv, in good agreement with the results of *Gasparin et al*. [2012] from the FLUSEC campaign data.

The maximum transports are seen from May to June and October. In contrast to the St George Channel, the minimum transport is located in March. The interannual variability of the transport through this section is interestingly well correlated to that at Solomon Strait (Figure 7h). This would demonstrate that a climatic modulation of the SEC input is primarily transmitted to Solomon Strait rather than to Vitiaz Strait or St George's Channel, favoring this route to the EUC.

An overall balance of the transports in and out of the Solomon Sea is given in Figure 8. Numbers are provided for both the transports between the surface and 300 m depth and for the whole depth. To the accuracy of our computations, the depth integrated transport through the south entrance of the Solomon Sea is balanced by the depth integrated transport in and out the straits. However, the transport is unbalanced for the surface flows and this could be a result of vertical water masses exchanges. The actual unbalance is of $\sim$1 Sv at the surface. The correlation between the transports through the southern section and the transports through the four Vitiaz, St George, Solomon, and Indispensable Straits is also indicated in Figure 8. This clearly shows that modulations of the southern section input are strongly reflected in the variability of the Vitiaz and Solomon Straits transports and not in the two other ones.

3.4. The Hypothetical SICU

The Solomon Islands Undercurrent (SICU) is the name given to a subsurface western boundary current flowing along the eastern side of the Solomon Islands. Its existence has been first evoked by *Kessler and Gourdeau* [2007] and then in the model study by *Melet et al*. [2010b].

To further explore this potential current, the time evolution of the transports through several cross sections east of the Solomon Islands has been examined. One example is shown in Figure 9 for the section extending from 155°E, 5.6°S to 156.3°E, 4.6°S. It is indeed found that there is a jet core at $\sim$200 m flowing northward. Between 100 and 300 m depth, the northward transport is $\sim$1 Sv. The location and the amplitude of this current correspond to that found by *Melet et al*. [2010b] for the SICU. However, a noticeable difference from the modeling study of *Melet et al*. [2010b] is that in the present 1/36° model, the potential SICU is significantly variable over time: a relatively strong equatorward coastal current in the 100–300 depth range

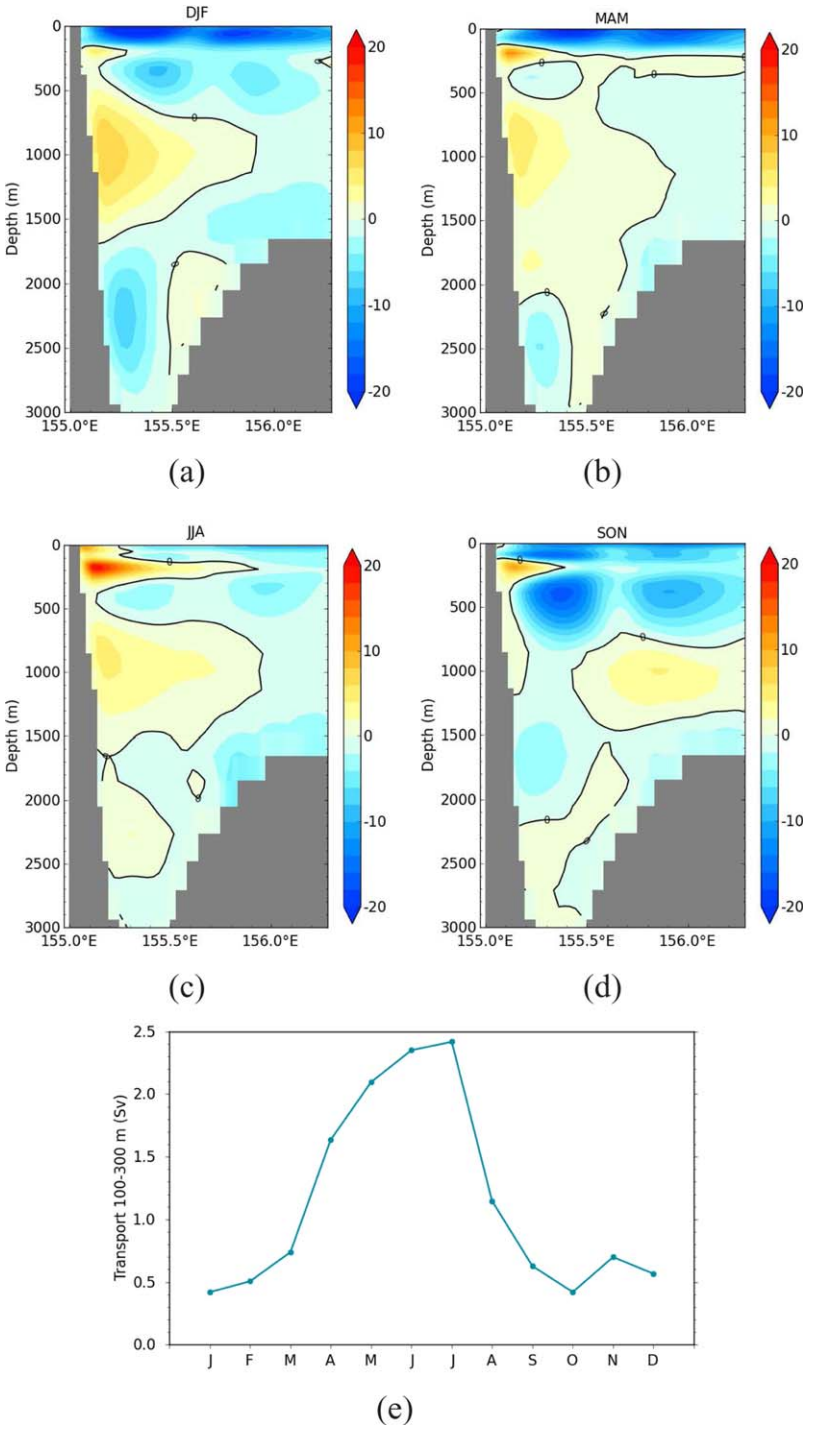

Figure 9. Velocity sections of the meridional flow in a section east of the Solomon Islands (dotted black line in Figure 8) and characterizing the SICU for the (a–d) four seasons and (e) seasonal cycle of transport (in Sv). Velocity scale is cm s^{-1}.

(exceeding 20 cm s^{-1}) is obtained from March to August whereas it is relatively weak (~2–8 cm s^{-1}) in September to February.

In our model, this current is very similar in terms of transport and location to what was observed during the PANDORA campaign in July 2012 (G. Eldin, personal communication, 2013). To our knowledge, there is no observation so far that would support the fact that the SICU could be permanent and the hypothesis supported by the present 1/36° model that it could be only a seasonal current deserves consideration. The

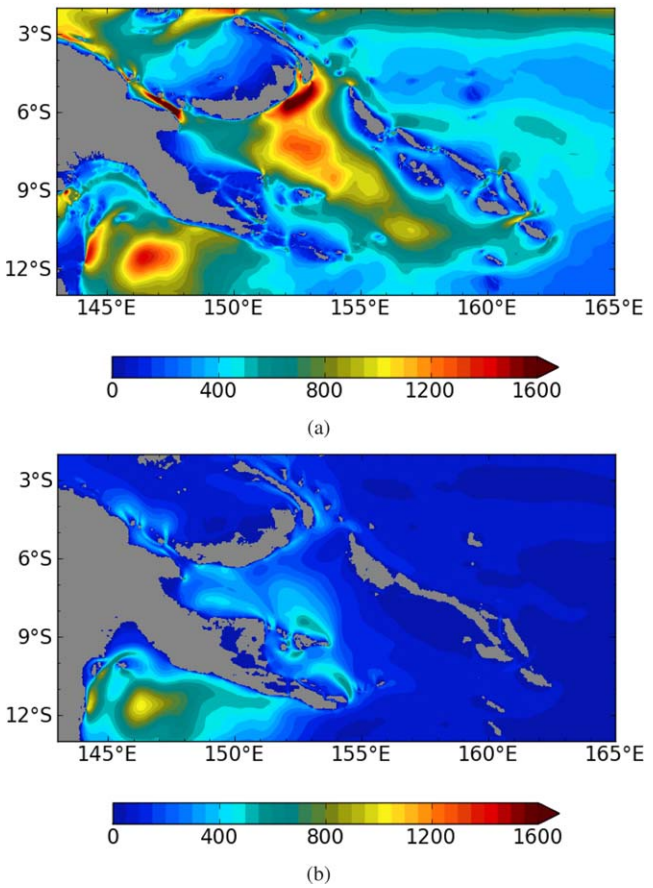

Figure 10. EKE fields ($cm^2 s^{-2}$) at (a) 10 m and (b) over the 200–300 m range averaged over the 1993–2007 period.

existence of a consistent western boundary undercurrent along the eastern coast of the Solomon Islands, such as the SICU, therefore remains uncertain.

Moreover, and more importantly in terms of transport than the SICU, a secondary northward current is simulated at depth (∼1000 m), which is in agreement with the jet structures discussed by *Cravatte et al.* [2012] as identified from ARGO floats.

A secondary jet is also observed in December-January-February at a depth of ∼2000 m in the reverse direction (poleward) and with a lesser magnitude in March-April-May.

4. Eddy Variability: An Eddy Kinetic Energy View

The Solomon Sea is a region of strong activity at scales of about 10–100 km and 10–100 days. These mesoscales and at least partly submesoscales are characterized by a large variety of dynamical features such as eddies, filaments, fronts, and waves. At this stage of our knowledge, it is very difficult to discriminate between the different dynamical mechanisms that can generate these features in the Solomon Sea since they likely result from a combination of different sources and instability processes. The large scale circulation feeding the Solomon Sea is a source of mesoscale activity (in particular the SEC inflow through Solomon Strait) but intrinsic features within the sea also induce eddy variability through instabilities of the LLWBCs themselves, topography effects, local baroclinic instabilities, shear effects at straits, etc. The recent work by *Gourdeau et al.* [2014] provides a first characterization of coherent mesoscale eddies in this area, but a lot remains to be done for the study of the mesoscale activity in the Solomon Sea.

It is known that the mesoscale features contain a large fraction of the energy of the ocean. The increase in resolution of the numerical model gives access to mesoscales and smaller scales and leads to an improved representation of scales interactions and corresponding transfers of energy both from the larger to smaller scales (direct cascade of energy) and from the smaller to the larger scales (inverse cascade of energy).

Moreover, the Solomon Sea region presents the highest levels of sea level variability of the whole tropical South Pacific Ocean. The sea level anomalies provided by the model have strong similarities with SLA products provided by altimeter data provided by AVISO (not shown). However, the AVISO resolution (1/3°) cannot faithfully represent the detailed SLA field and many bathymetric features are discarded during the gridding of altimetric data. As shown by *Melet et al.* [2010a], using AVISO data and their 1/12° numerical model, the variability in the Solomon Sea is associated with high levels of Eddy Kinetic Energy (EKE). Here the EKE fields are also considered as a relevant proxy for the eddy activity in our 1/36° model.

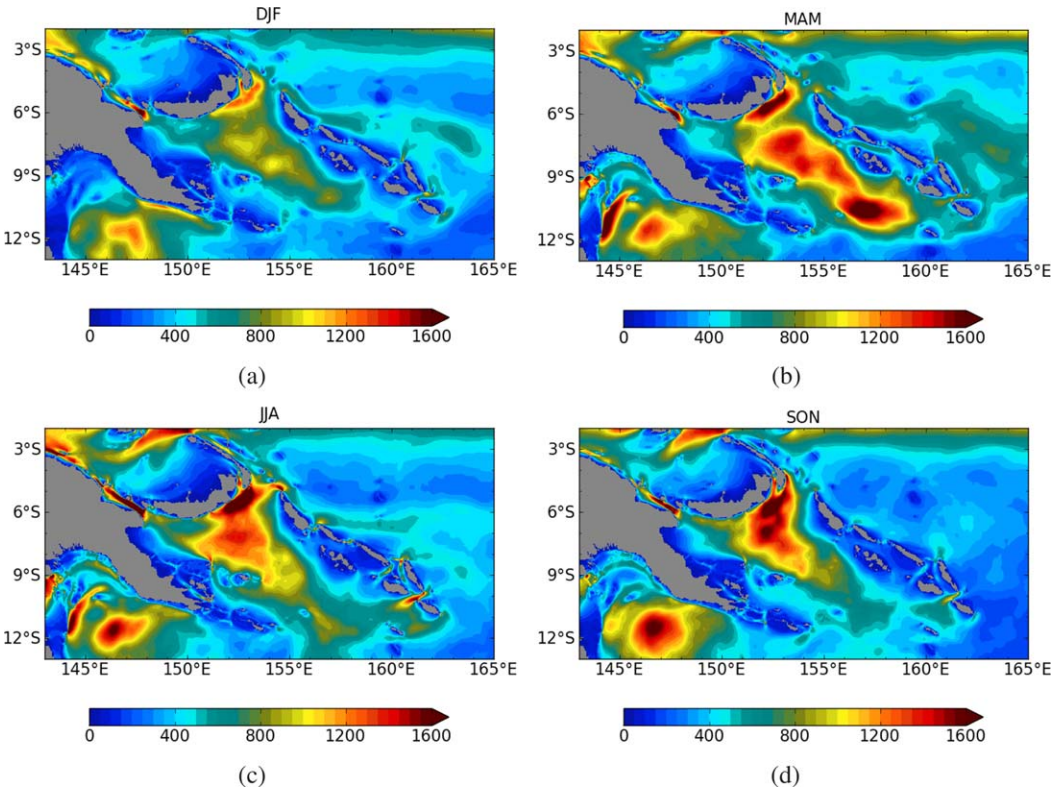

Figure 11. Seasonal variability of surface (10 m) EKE fields ($cm^2 s^{-2}$) averaged over the 1993–2007 period.

4.1. Mean EKE

EKE is classically computed as $1/2[(u-\bar{u})^2+(v-\bar{v})^2]$ and averaged here over the 1993–2007 period. This computation is based on daily resolution, where daily velocity (u, v) anomalies are referenced to monthly mean velocity fields $(\bar{u}, \bar{v})$. The EKE field at 10 m is shown in Figure 10a. A patch of high variability is observed west of Solomon Strait with an amplitude of nearly 1600 $cm^2\ s^{-2}$, which is equivalent to a rms velocity anomaly of 40 cm s^{-1}. These EKE values are typical of those observed within the western boundary currents at midlatitudes. Contrary to the surface layer, the EKE in subsurface layers (over 200–300 m depth) is small in the eastern part of the Solomon Sea (Figure 10b). At this depth, a strong signature of EKE is still found within the Solomon Sea, but it is clearly connected to the variability of the NGCU and within the Gulf of Papua, where the variability of the GPC is intense.

Figure 10a clearly shows that within the Solomon Sea the high level of EKE is associated with regions of strong horizontal and vertical shears that were already observed in the circulation patterns. Vitiaz, St George's, Solomon, and Indispensable Straits are locations of intense very localized EKE burst that are the signature of high variability.

The 1/36° model has a mean level of EKE that is approximately 30–40% larger than in the 1/12° model. This large difference is seen not only at the surface but at all depths. This result clearly points out the impact of the increased resolution on the energy budget.

4.2. Seasonal Variability

There is a clear seasonal cycle of surface EKE as can be seen in Figure 11. The analysis of surface EKE from Lagrangian drifters data by *Hristova and Kessler* [2011] showed maximum values from April to June and minimum values from August to December. Within the Solomon Sea, the seasonal analysis of the surface EKE variability from the 1/36° model showed maximum values from March to May and minimum values from December to February. These modeling results are in good agreement with the observational results of *Hristova and Kessler* [2011].

Figure 11 also shows that the March to April to May period corresponds to a high variability season within the Solomon Sea, and to a less extent east of the Solomon Islands. Analysis of the velocity field shows that

the high EKE level at the entrance of Solomon Strait is associated with the westward SEC that flows through Solomon Strait and into the Solomon Sea during this period (as it is also evidenced in *Gourdeau et al.* [2014]). The location of the maximum of variability changes with seasons according to *Hristova and Kessler* [2011].

East of the Solomon Islands, the relatively large EKE signal likely reflects the enhanced eddy activity generated through barotropic instability of the SEC-SECC (South Equatorial Counter Current) system [*Qiu and Chen*, 2004; *Hristova and Kessler*, 2011], with maximum EKE values in March-April-May and minimum EKE values in September-October-November.

Within the 200 to 300 m depth range, the EKE seasonal variability (not shown) is still remarkable although it is lower than at the surface. The location of the patch of maximum variability inside the Solomon Sea is slightly shifted westward relative to the one observed at surface, with values reaching 500 $cm^2\ s^{-2}$ (which is equivalent to a rms velocity anomaly of $\sim$22 $cm\ s^{-1}$). The EKE signature over this 200 to 300 m range of depth within the Solomon Sea seems to match the location of the NGCU. It likely reflects the instabilities of the NGCU. North of the Woodlark Islands, the EKE field is more widely spread.

5. Mesoscale and Submesoscale: A Spectral View

All the previous findings indicate that the 1/36° resolution model of the Solomon Sea provides a realistic picture of the actual circulation in the sea (at least with regard to existing observations) and that a major increase in the levels of variability is evidenced. This is associated with a better resolution of the variability features that populate this area.

Together with the clear signature of a number of mesoscale features, the emergence of smaller submesoscales is apparent. The wealth of small-scales structures can be easily seen through the relative vorticity field of Figure 12a, for example. This surface relative vorticity field reveals many small features such as frontogenesis stretching stirring process, filaments, or even small coherent vortices of typically 10–40 km (that are certainly not well resolved by the model but that are "permitted" to be resolved by the model). The same small features can also be seen on salinity (Figure 12b) and temperature (Figure 12c).

The Solomon Sea straits are a source of mesoscale and submesoscale variability and/or the location of strong eddy fluxes as can be seen for example in Figures 13a (near Indispensable Strait) and 13b (through Solomon Strait). Straits geometry partly controls the scaling of the variability features. Bathymetry in general may be the source of variability and there are many examples looking for instance at relative vorticity movies of our simulation showing the generation of small scale eddies over seamounts or in the lee of many islands.

A careful examination of all these features requires a detailed analysis and is not possible in the framework of the present paper. This will be the subject of further investigations from these complex regional simulations. Looking at the eddy activity in the Solomon Sea has been approached recently by *Gourdeau et al.* [2014] from a 1/12° only resolution numerical model. At this stage, we decided to approach the problem in a rather synoptical way, using the tools of several recent works on submesoscales.

5.1. Spectral Analysis

Turbulence theories applied to the studies of mesoscale and submesoscale dynamics provide powerful theoretical frameworks and tools. Spectral analysis is often performed to characterize the variance of oceanic processes at different scales and transfers of energy between different scales. Two approaches are commonly used today to study dynamics at mesoscales and submesoscales: the quasigeostrophic (QG) and surface quasigeostrophic (SQG) theories. The quasigeostrophic turbulence paradigm was originally proposed by *Charney* [1971]. In the QG theory, the inverse cascade is characterized by a k^{-3} power law for the kinetic energy spectrum (k is the wave number) leading to a k^{-5} power law for the SSH spectrum. In the SQG theory [*Blumen*, 1978], the same inverse cascade would follow a $k^{-5/3}$ power law for the kinetic energy spectrum and a $k^{-11/3}$ power law for the SSH spectrum.

Using altimetric data, *Stammer* [1997] suggests that the sea level spectrum computed in regions of high KE compares well with the QG turbulence model. The recent study of *Le Traon et al.* [2008], using the most recent altimetric data set, shows that slopes of SSH spectrum are in fact closer to a $k^{-11/3}$ power law, which is in favor of the SQG turbulence theory. The difference of results may be due to the limitation in spatial resolution of observations.

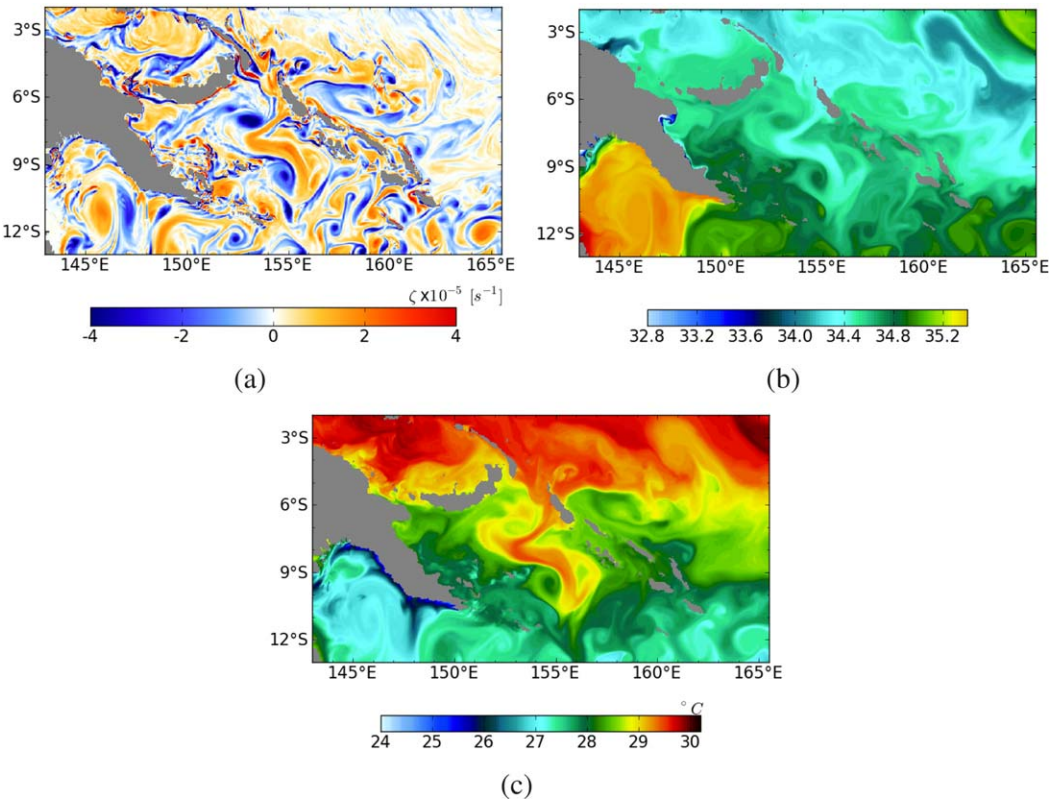

Figure 12. Example of surface relative (a) vorticity, (b) salinity, and (c) temperature fields on 9 November 1994. Blue and orange crosses correspond, respectively, to cyclonic and anticyclonic eddies.

The motivation of what follows is to take advantage of the high-resolution model of the Solomon Sea to study mesoscale and submesoscale turbulence dynamics, and the way the energy is transferred between different scales. Therefore, wave number spectral analysis is performed and spectral slopes are characterized. Kinetic spectral fluxes are also evaluated.

5.2. Wave Number SSH, SST, and KE Spectra

SSH, SST, and KE wave number spectra are estimated in two-dimensional boxes characterizing various dynamical situations in the Solomon Sea region. The location of the boxes A, B, and C is shown in Figure 14g.

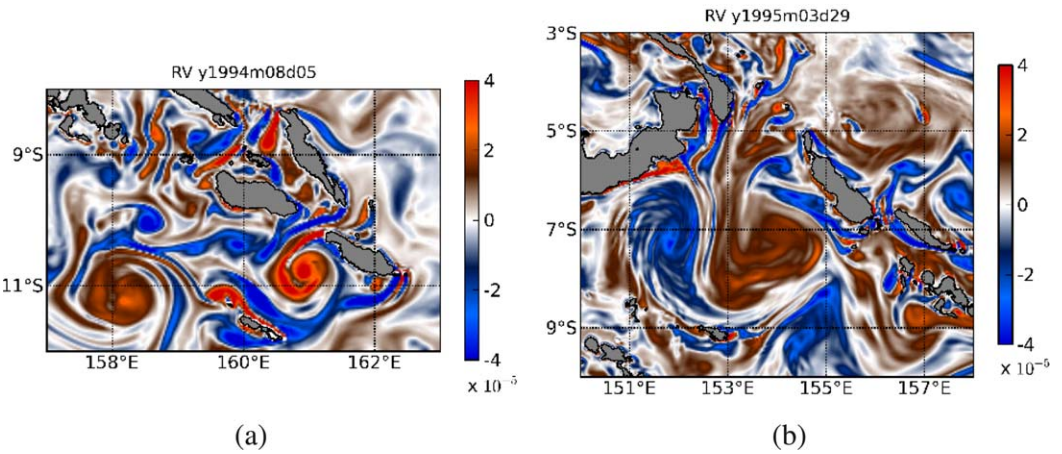

Figure 13. Examples of relative vorticity fields showing small structures in vicinity of (a) Indispensable Strait and (b) large mesoscales features entering Solomon Strait.

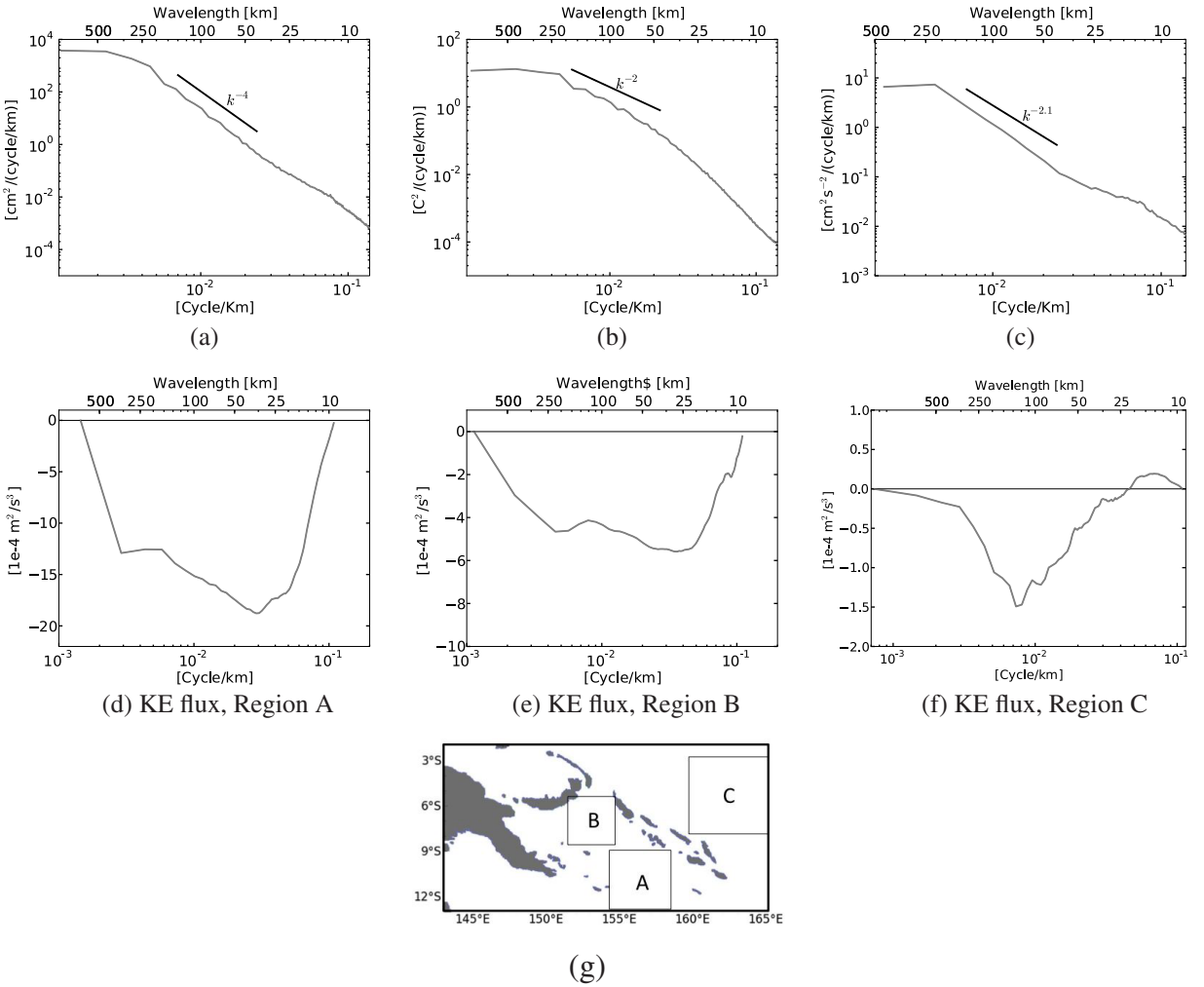

Figure 14. SSH, SST, and KE wave number spectrum for (a–c) box A and KE fluxes for (d) box A, (e) box B, and (f) box C. (g) Locations of boxes A, B, and C.

Due to the complicated topography of the Solomon Sea, the boxes considered here are not as large as the ones used in the studies of *Richman et al.* [2012], *Sasaki and Klein* [2012], and *Xu and Fu* [2011], but were chosen to be large enough to contain significant mesoscale and submesoscale features. As mentioned previously, the bathymetry of the Solomon Sea is very complicated. For this reason, it would not be reliable to consider wider domains for the spectral analysis because of the numerous small islands that could spuriously disturb the signal when applying a Fourier transform. The choice and the geometry of the zones of interest are determined so that they both take into account the physical limits that are imperatively imposed by the islands, but also include as much as possible the extent of the eddy-activity. In addition, due to the geometrical constraints, the boxes does not strictly have the same size. For this study, boxes are considered over three domains that are energetically contrasted: the first one is located at the south entrance of the Solomon Sea (box A), the second one is located inside the Solomon Sea (box B) and finally, the third one is located east of the Solomon Sea (box C). At the entrance of the Solomon Sea, box A encompasses a region of low EKE. Box B is located over a high EKE region and box C is located in a low EKE region where the SEC flows. The Fourier decomposition required for the spectral analysis is performed on regions with 150 × 150, 112 × 112, and 220 × 220 grid points corresponding to boxes A, B, and C, respectively. Daily output fields are used to compute the SSH, SST, and KE spectrum. The daily spectra are then averaged over 2 years (1995–1996) to produce a mean spectrum of SSH, SST, and KE for each box. Let us point out these two considered years are not characteristic of ENSO events: they are intentionally chosen as "normal" years to avoid impacts of particular ENSO events.

SSH, SST, and KE spectra are computed as a function of the horizontal wave number magnitude after azimutal integration in wave number space. SSH and SST fields are made doubly periodic in both zonal and meridional directions by doubling boxes size in the same way as in *Lapeyre* [2009] and *Sasaki and Klein* [2012] to allow Fourier analysis of the nonperiodical signal. The signals were then detrended before computing Fourier transforms. Let us mention in addition that here, KE is computed (contrary to the previous section 4) from the geostrophic velocity field derived from the SSH field and not from the full velocity. This is motivated by the willingness to adopt the same computing approach than the studies by *Richman et al*. [2012], *Sasaki and Klein* [2012], and *Xu and Fu* [2011] in order to compare to their results. However, contrary to *Xu and Fu* [2011], the mesoscale band was not restricted to 70–250 km to estimate the spectrum slope since we are not constrained as they were, by the specific nature (and the noise level) of altimetric data.

Figures 14a–14c give examples of the SSH, SST, and KE wave number model spectra, respectively, for the only box A. The results are similar for boxes B and C and were not found useful to present. The SSH wave number spectra follow a k^{-4} slope in all boxes. This slope is close to that predicted from the SQG turbulence theory and is consistent with the results of *Sasaki and Klein* [2012] and *Richman et al*. [2012]. For the SST, the computed wave number slope is of the order of k^{-2}. This result corroborates those of *Sasaki and Klein* [2012]. Finally, for the KE, the spectrum slope is found to be of order k^{-2} for the three boxes, which is again consistent with results of *Sasaki and Klein* [2012].

This compliance of the model spectra with the SQG theory is seen as a strong result that was not fully expected given the previous findings in low latitudes by *Xu and Fu* [2011].

Beyond this specific point on SQG theory, one other key point here is that an inverse cascade is active even from quite small scales, highlighting the actual dynamical impact of small scales on the larger scales.

5.3. Kinetic Energy Spectral Flux

Ocean dynamics is strongly nonlinear in the Solomon Sea and is characterized by intense interactions and transfers of energy between scales. To study how energy is transferred between different spatial scales, the KE spectral flux Π (which is the flux of energy through wave numbers) is computed. This flux arises in particular through the advective terms of the momentum equations. Precisely, it is computed as the integral of the local horizontal advective term from the wave number k to the largest wave number k_{max} [e.g., *Scott and Wang*, 2005; *Sasaki and Klein*, 2012]:

$$\Pi(k)=\int_{k}^{k_{max}} -\mathbb{R}\left[\widehat{u_g}^{*}.\left(\widehat{u_g.\nabla_h u_g}\right)\right](k)dk, \tag{1}$$

where u_g is the horizontal geostrophic velocity field estimated from the SSH, ∇_h is the horizontal gradient operator, and k_{max} is the wave number corresponding to the grid size. The caret indicates the horizontal spectral transform, the asterisk notation is the complex conjugate and $\mathbb{R}$ is the real part of the Fourier transform. For this computation, the same doubly periodic boxes as in the spectral analysis above are considered [*Sasaki and Klein*, 2012].

Similarly to the spectra computation, the spectral KE fluxes are computed from daily fields over the 1995–1996 period and a mean spectral kinetic energy flux is then produced. In both boxes A and B (Figures 14a and 14b), the KE spectral flux is predominantly negative, which indicates a predominantly inverse cascade. This result also shows that the kinetic energy is transferred from smaller to larger scales within a large spectral range. In box C (Figure 14c), the kinetic energy spectral flux changes sign at the wave number corresponding to a physical scale of 25 km. From this wave number, there is a negative kinetic energy spectral flux toward larger scales and a positive flux toward smaller scales. In other terms, both an inverse energy cascade toward large scales and a direct (dissipative) energy cascade toward smaller scales are observed in this region. It is interesting to see in this later case the coexistence of the two cascades, and in particular to observe a direct cascade below 25 km. In addition, 25 km marks the limit of the model resolution based on the notion of effective resolution [*Skamarock*, 2004; *Marchesiello et al*., 2011]. Indeed, 25 km in the Solomon Sea region corresponds to $\sim 8\delta x$ (that roughly give an estimate of the effective resolution in numerical models), where δx is the horizontal nominal resolution (which is $\sim$3 km in this model).

Overall, these KE flux computations clarify what range of scales, including small scales, experiences an inverse energy cascade.

6. Conclusion

A 1/36° high-resolution model configuration has been developed in order to provide a consistent scheme of the Solomon Sea circulations. The circulations in the Solomon Sea are of importance since this region represents a transit area for the South Pacific Low Latitude Western Boundary Current flowing from the subtropics to the equatorial Pacific. When compared to available observations, the model surface and thermocline circulations proved to be quite realistic [e.g., *Lindstrom et al*., 1987, 1990; *Kessler and Gourdeau*, 2007; *Maes et al*., 2009; *Cravatte et al*., 2011; *Hristova and Kessler*, 2011; *Gasparin et al*., 2012; *Kessler and Cravatte*, 2013]. With regard to the previous simulations of *Melet et al*. [2010b], improvements are seen for the main pathway of the NGCU within the Solomon Sea around the Woodlarks Islands. Significant differences are observed for the current structure east of the Solomon Sea: while the model captures the NICU along the eastern coast of the island of New Ireland, along the eastern coasts of the Solomon Islands, the model simulates a seasonally intermittent SICU. Several other detailed features in relation to bathymetric signature are also improved or modified but it is difficult at this stage to assess their validity as the needed corresponding observations are missing. The flows through the straits of the Solomon Sea are important for determining the different equatorward pathways of the Solomon Sea waters. A faithful representation of such flows is therefore important and a detailed analysis of flows through straits has been carried out.

Overall the Solomon Sea circulation patterns from the 1/36° model are consistent with the literature. The process is "convergent" in the sense that new findings do not contradict, but rather refine and improve the existing picture of those circulations and of the western boundary routes from the subtropics to the equator. The SICU might be one exception if the 1/36° model result in this regard is confirmed by future specific observations.

Our high-resolution model simulation provides very complex and rich information about the Solomon Sea circulations, such that it raises specific issues for the analysis, not only in terms of computing constraints. Indeed, defining a good strategy for analysis and diagnostics becomes far from straightforward. The richness of the model information is only very partially compliant with observations. It is thought that a back and forth interaction strategy might be built between model and observations to clarify several physical points the priority of which is not necessarily clear at first sight. We believe that this will become more and more an issue as increasingly high-resolution and complex models will be developed without the concomitant observational database.

The 1/36° model simulation exhibits an intense variability at the mesoscales and some variability at the submesoscales is also clearly obtained. A striking result is the increase by 30–40% in the level of eddy kinetic energy observed everywhere, including at depth, with regard to the numbers that were obtained with the 1/12° resolution model. The overall level and seasonal cycle of the surface model eddy kinetic energy within the Solomon Sea are in agreement with altimetric satellite and with drifter observations [*Melet et al*., 2010a; *Hristova and Kessler*, 2011]. At the surface, the variability distribution seems quite well related to horizontal and/or vertical shears of the currents and/or bathymetric features. For the subsurface, the variability seems to be more related to instabilities of the New Guinea Undercurrent.

We have taken advantage of having a 1/36° relatively fine resolution to explore smaller scales in the Solomon Sea. This includes submesoscale eddies and filaments associated to mesoscale eddies interaction but also many features that are in relation with the complex bathymetry of this region. Several high-resolution numerical model simulations have been analyzed for wave number spectral slopes in some more or less energetic regions of the world ocean [*Capet et al*., 2008; *Sasaki and Klein*, 2012; *Richman et al*., 2012]. In the present 1/36° resolution model simulations, the SSH wave number spectrum has a slope of k^{-4} in the three boxes under consideration even though they are quite distinct dynamically and energetically. On the other hand, the kinetic energy spectrum of the model exhibits a slope of k^{-2}. These results do not compare well with the results of *Xu and Fu* [2011] but rather are more consistent with studies by *Sasaki and Klein* [2012] and close to the predictions of the SQG turbulence theory.

In this study, the slope of spectrum does not vary a lot between the three different boxes that have been considered. In particular, there is not a clear difference for the spectrum slopes in regions of low EKE relatively to region of high EKE. In all situations, inverse cascades are characterized even at small scales than showing a clear impact of small scales on larger scales. This is another important result of this work together with the agreement with the SQG theory.

One could have expected some difficulties based on the fact that previous turbulence theories assume an isotropic fluid. Yet, the complexity of the Solomon Sea domain and of the bathymetry together with the actual anisotropy of the Solomon Sea circulation could have made the assumption irrelevant in this region. Nevertheless, the wave number spectrum from the 1/36° model does not seem to be strongly impacted by the anisotropy of the oceanic conditions in the Solomon Sea and provide results that are close to those turbulence theories.

Clearly, our results are limited by the model shortcomings. For instance, the model does not take into account (or properly resolve) some important physical processes, especially tides and internal waves. We also critically lack an observational database to more carefully assess the model results and deficiencies. Further work should be done in these two directions together. On the short term, the results of the dedicated PANDORA campaign should provide valuable additional observations [*Eldin et al.*, 2013].

Acknowledgments

This research has been conducted with the support of the Centre National d'Etudes Spatiales (CNES) and of the Centre National de la Recherche Scientifique (CNRS). This work was granted access to HPC resources under the allocations x2012–010727 and x2013–010727 attributed by GENCI (Grand Equipement National de Calcul Intensif) to the DRAKKAR project, simulations being carried out at both the IDRIS and CINES supercomputer facilities. The data for this paper are available at DRAKKAR project (www.ifremer.fr/lpo/drakkar).

References

Adcroft, A., C. Hill, and J. Marshall (1997), Representation of topography by shaved cells in a height coordinate ocean model, *Mon. Weather Rev.*, *125*, 2293–2315.

Barnier, B., et al. (2006), Impact of partial steps and momentum advection schemes in a global ocean circulation model at eddy-permitting resolution, *Ocean Dyn.*, *56*(5–6), 543–567.

Blumen, W. (1978), Uniform potential vorticity flow: Part I. Theory of wave interactions and two-dimensional turbulence, *J. Atmos. Sci.*, *35*, 774–783.

Butt, J., and E. Lindstrom (1994), Currents off the east coast of New Ireland, Papua New Guinea, and their relevance to regional undercurrents in the western Equatorial Pacific Ocean, *J. Geophys. Res.*, *99*, 12,503–12,514.

Capet, X., J. C. McWilliams, M. J. Molemaker, and A. Shchepetkin (2008), Mesoscale to submesoscale transition in the California current system. Part I: Flow structure, eddy flux, and observational tests, *J. Phys. Oceanogr.*, *38*, 29–43.

Chang, P., Y. Fang, R. Saravanan, L. Ji, and H. Seidel (2006), The cause of the fragile relationship between the Pacific El Niño and the Atlantic Niño, *Nature*, *443*, 324–328.

Charney, J. G. (1971), Geostrophic turbulence, *J. Atmos. Sci.*, *28*, 1088–1095.

Cravatte, S., A. Ganachaud, Q.-P. Duong, W. S. Kessler, G. Eldin, and P. Dutrieux (2011), Observed circulation in the Solomon Sea from SADCP data, *Prog. Oceanogr.*, *88*, 116–130.

Cravatte, S., W. S. Kessler, and F. Marin (2012), Intermediate zonal jets in the tropical Pacific Ocean observed by Argo floats, *J. Phys. Oceanogr.*, *42*, 1475–1485.

Davis, R. E., W. S. Kessler, and J. T. Sherman (2012), Gliders measure western boundary current transport from the south pacific to the equator, *J. Phys. Oceanogr.*, *42*, 2001–2013.

Debreu, L., C. Vouland, and E. Blayo (2008), AGRIF: Adaptive grid refinement in Fortran, *Comput. Geosci.*, *34*, 8–13.

Dee, D. P., et al. (2011), The ERA-interim reanalysis: Configuration and performance of the data assimilation system, *Q. J. R. Meteorol. Soc.*, *137*(656), 553–597.

Djath, B., A. Melet, J. Verron, J.-M. Molines, B. Barnier, L. Gourdeau, and L. Debreu (2014), A 1/36° model of the Solomon Sea embedded into a global ocean model: On the setting up of an interactive open boundary condition nested model system, *J. Oper. Oceanogr.*, *7*(1), 34–46.

Eldin, G., A. Ganachaud, S. Cravatte, and C. Jeandel (2013), Pandora cruise provides an unprecedented description of the Solomon Sea, *CLIVAR Newsl. Exch.*, *61*(18), 24–25.

Fedorov, A., and S. Philander (2001), A stability analysis of tropical ocean-atmosphere interactions: Bridging measurements and theory for El Nino, *J. Clim.*, *14*, 3086–3101.

Fine, R. A., R. Lukas, F. Bingham, M. Warnar, and R. Gammon (1994), The western equatorial Pacific: A water mass crossroads, *J. Geophys. Res.*, *99*, 25,063–25,080.

Fu, L. L., D. Alsdorf, E. Rodriguez, R. Morrow, N. Mognard, J. Lambin, P. Vaze, and T. Lafon (2009), The SWOT (Surface Water and Ocean Topography) mission: Spaceborne radar interferometry for oceanographic and hydrological applications, paper presented at *OceanObs'09*, NASA/CNES, Venice, Italy, 21–25 September.

Ganachaud, A., et al. (2013), Advances from the Southwest Pacific Ocean Circulation and Climate Experiment (SPICE), *Tech. Rep. 61*, vol. 18, CLIVAR Exch., Legos/France.

Gasparin, F., A. Ganachaud, C. Maes, F. Marin, and F. Eldin (2012), Oceanic transports through the Solomon Sea: The bend of the New Guinea coastal undercurrent, *Geophys. Res. Lett.*, *39*, L15608, doi:10.1029/2012GL052575.

Gourdeau, L., J. Verron, A. Melet, W. Kessler, F. Marin, and B. Djath (2014), Exploring the mesoscale activity in the Solomon Sea: a complementary approach with numerical model and altimetric data, *J. Geophys. Res. Oceans*, *119*, 2290–2311, doi:10.1002/2013JC009614.

Hristova, H. G., and W. S. Kessler (2011), Surface circulation in the Solomon Sea derived from Lagrangian drifter observations, *J. Phys. Oceanogr.*, *42*, 448–458.

Kessler, W. S., and S. Cravatte (2013), ENSO and short-term variability of the South Equatorial current entering the Coral Sea, *J. Phys. Oceanogr.*, *43*, 956–969.

Kessler, W. S., and L. Gourdeau (2007), The annual cycle of circulation of the southwest subtropical Pacific, analyzed in an ocean GCM, *J. Phys. Oceanogr.*, *37*, 1610–1627.

Lapeyre, G. (2009), What vertical mode does the altimeter reflect? On the decomposition in baroclinic modes and on a surface-trapped mode, *Am. Meteorol. Soc.*, *39*, 2857–2874, doi:10.1175/2009JPO3968.1.

Large, W., and S. Yeager (2009), The global climatology of an interannually varying air-sea flux data set, *Clim. Dyn.*, *33*, 341–364.

Le Traon, P. Y., P. Klein, B. L. Hua, and G. Dibarboure (2008), Do altimeter wavenumber spectra agree with interior or surface quasigeostrophic theory?, *J. Phys. Oceanogr.*, *38*, 1137–1142.

Levitus, S., T. Boyer, M. Conkright, T. O. Brien, J. Antonov, C. Stephens, L. Stathoplos, D. Johnson, and R. Gelfeld (1998), *NOAA Atlas NESDIS 18, World Ocean Database 1998*, vol. 1, *Introduction*, technical report N° 18, 346 pp., U.S. Gov. Print. Off., Washington, D. C.

Lindstrom, E., R. Lukas, R. Fine, E. Firing, S. Godgrey, G. Meyers, and M. Tsuchiya (1987), The western equatorial ocean circulation study, *Nature*, *330*, 533–537.
Lindstrom, E., J. Butt, R. Lukas, and S. Godfrey (1990), The flow through Vitiaz Strait and St Georges's Channel, Papua New Guinea, in *The Physical Oceanography of Sea Strait*, pp. 171–189, Kluwer Acad., Netherlands.
Madec, G. (2008), NEMO ocean engine, Note du Pole de Modélisation, *Tech. Rep. 27*, 300 pp., Inst. Pierre Simon Laplace, France.
Maes, C., G. Eldin, A. Melet, J. Lefèvre, J. Sudre, D. Varillon, A. Ganachaud, and L. Gourdeau (2009), Rapport de la mission océanographique FLUSEC-01 à bord du N.O. Alis du 12 au 30 Août 2007 en mer de Corail, Océan Pacifique Sud-Ouest, *Rapp. Missions 24*, IRD (Institut de Recherche pour le Développement), Nouméa.
Marchesiello, P., X. Capet, C. Menkes, and S. C. Kennan (2011), Submesoscale dynamics in tropical instability waves, *Ocean Modell.*, *39*, 31–46.
Melet, A., L. Gourdeau, and J. Verron (2010a), Variability of the Solomon Sea circulation from altimetry sea level data, *Ocean Dyn.*, *60*(4), 883–900.
Melet, A., L. Gourdeau, W. Kessler, J. Verron, and J. Molines (2010b), Thermocline circulation in the Solomon Sea: A modeling study, *J. Phys. Oceanogr.*, *40*, 1302–1319.
Melet, A., J. Verron, L. Gourdeau, and A. Koch-Larrouy (2011), Solomon Sea water masses pathways to the equator and their transformations, *J. Phys. Oceanogr.*, *41*, 810–826.
Melet, A., L. Gourdeau, J. Verron, and B. Djath (2013), Solomon Sea circulation and water mass modifications: Response at ENSO timescales, *Ocean Dyn.*, *63*, 1–19.
Morrow, R., and P. Le Traon (2012), Recent advances in observing mesoscale ocean dynamics with satellite altimetry, *Adv. Space Res.*, *50*, 1062–1076.
Murray, S., E. Lindstrom, J. Kindle, and E. Weeks (1995), Transport through Vitiaz Strait, WOCE Notes *7*, U.S. WOCE Off., College Station, Tex.
Qiu, B., and S. Chen (2004), Seasonal modulations in the eddy field of the South Pacific ocean, *J. Phys. Oceanogr.*, *34*, 1515–1527.
Richman, J. G., B. K. Arbic, J. F. Shriver, E. J. Metzger, and A. J. Wallcraft (2012), Inferring dynamics from the wavenumber spectra of an eddying global ocean model with embedded tides, *J. Geophys. Res.*, *117*, C12012, doi:10.1029/2012JC008364.
Ridgway, K. R., J. R. Dunn, and J. L. Wilkin (2002), Ocean interpolation by weighted least squares: Application to the waters around Australia, *J. Atmos. Oceanic Technol.*, *19*, 1357–1375.
Sasaki, H., and P. Klein (2012), SSH wavenumber spectra in the North Pacific from a high-resolution realistic simulation, *J. Phys. Oceanogr.*, *42*, 1233–1241.
Scott, R. B., and F. Wang (2005), Direct evidence of an oceanic inverse kinetic energy cascade from satellite altimetry, *J. Phys. Oceanogr.*, *35*, 1650–1666.
Skamarock, W. C. (2004), Evaluating mesoscale nwp models using kinetic energy spectra, *Mon. Weather Rev.*, *132*, 3019–3032.
Stammer, D. (1997), Global characteristics of ocean variability estimated from regional topex/poseidon altimeter measurements, *J. Phys. Oceanogr.*, *27*, 1743–1769.
Sun, D., T. Zhang, and S. Shin (2004), The effect of subtropical cooling on the amplitude of enso: A numerical study, *J. Clim.*, *17*, 3786–3798.
Tréguier, A. M., B. Barnier, A. P. de Miranda, J. M. Molines, N. Grima, M. Imbard, G. Madec, C. Messager, T. Reynaud, and S. Michel (2001), An eddy-permitting model of the Atlantic circulation: Evaluating open boundary conditions, *J. Geophys. Res.*, *106*, 115–129.
Tsuchiya, M. (1981), The origin of the Pacific Equatorial 13°C water, *J. Phys. Oceanogr.*, *11*, 794–812.
Tsuchiya, M., R. Lukas, R. Fine, E. Firing, and E. Lindstrom (1989), Source waters of the Pacific Equatorial Undercurrent, *Prog. Oceanogr.*, *23*, 101–147.
Verron, J. (2013), SARAL/AltiKa: A Ka band altimetric mission, AVISO Newsl. 10, France.
Xu, Y., and L.-L. Fu (2011), Global variability of the wavenumber spectrum of oceanic mesoscale turbulence, *J. Phys. Oceanogr.*, *41*, 802–809.